Peer-reviewed version available at Coatings 2017, 7, 45; doi:10.3390/coatings7030045

Review

Review of Antibacterial Activity of Titanium-based Implants Surfaces Fabricated by Micro-arc Oxidation

Xiaojing He, Xiangyu Zhang *, Xin Wang and Lin Qin

College of Materials Science and Engineering, Taiyuan University of Technology, Taiyuan, China
* Correspondence: zhangxiangyu@tyut.edu.cn; Tel.: +86-351-601-0540

Abstract: Ti and its alloys are the most commonly used materials for biomedical applications. However, bacterial infection after implant placement is still one of the significant rising complications. Therefore, the application of the antimicrobial agents into implant surfaces to prevent implant-associated infection has attracted lots of attentions. Scientific papers have shown that inorganic antibacterial metal elements (*e.g.* Ag, Cu, Zn) can be introduced into implant surfaces with the addition of metal nanoparticles or metallic compounds into electrolyte via micro-arc oxidation (MAO) technology. In this review, the effects of the composition and concentration of electrolyte and process parameters (*e.g.* voltage, current density, oxidation time) on morphological characteristics (*e.g.* surface morphology, bonding strength), antibacterial ability and biocompatibility of MAO antimicrobial coatings were discussed in detail. Anti-infection and osseointegration can be simultaneously accomplished with the selection of the proper antibacterial elements and operating parameters. Besides, MAO assisted by magnetron sputtering (MS) to endow Ti-based implant materials with superior antibacterial ability and biocompatibility was also discussed. Finally, the development trend of MAO technology in the future was forecasted.

Keywords: Micro-arc oxidation; Antibacterial ability; Ag; Cu; Zn

1. Introduction

Biomedical titanium (Ti) and its alloys have been widely used in blood vessels, artificial joints, dental implantations and bone screws [1-3] on account of their excellent mechanical properties, good corrosion resistance and favorable biocompatibility. However, implant-associated infection (IAI) remains one of the most devastating postoperative complications [4,5] despite strict sterilization and systemic antibiotic prophylaxis prior to surgery. IAI often commences with bacterial adhesion to the implant and colonization on the implant surface, followed by biofilm formation. The biofilms are extraordinarily resistant to antibiotics and the host immunity defensive system [6-8], leading to further complications. Once the biofilms are formed, it is often not effectively treated except for prosthesis removal and re-implantation [9,10]. This devastating complication may result in chronic suffering and extremely huge medical expenses [11,12]. Therefore, it is highly desirable to introduce antimicrobial agents into implant surfaces to provide antibacterial activities and prevent peri-implant infections [13-17]. In comparison with organic antibiotics, inorganic antibacterial metal elements (*e.g.* silver (Ag)[18-22], copper (Cu)[23-26], and zinc (Zn)[27-29]) have attracted great attentions due to their perfect stabilities, superior broad-spectrum antibacterial properties, relatively low toxicity to human cells and low risk of producing resistant strains[30,31].

Dizaj *et al.*[32] have reviewed the antimicrobial activity of metal and metal oxide nanoparticles together with their antimicrobial mechanisms, and have indicated that the particle size determined the antimicrobial effectiveness of the metal nanoparticles. Rai *et al.* [33] have extensively reviewed the antibacterial, antifungal and antiviral properties of Ag ions, Ag compounds and Ag nanoparticles, but there is no discussion about the antibacterial properties of Cu or Zn. In addition, the toxicities of metal and metal oxide nanoparticles to apply as proper alternatives for antibiotics in biomedical applications were not discussed in the reviews. In order to obtain antibacterial metallic surfaces, numerous surface modifications have been performed. Ferraris *et al.* [34] have reported the

surface modification technologies such as ion implantation[35,36], ion beam assisted deposition[37], electrochemical techniques[38], ion exchange[39], sol–gel[40], sputtering[41,42], plasmas pray[43] and chemical vapour deposition[44]. However, micro-arc oxidation (MAO) is not fully described.

MAO, which can produce porous, adhesive and bioactive coatings for implantation, has aroused considerable attention [45-47]. On one hand, porous bioactive calcium phosphate-based composite layer can be deposited on Ti-based implant surfaces according to the selected electrolyte, which would enhance the biocompatibility[48,49] and the bonding strength of the coated layer[50]. On the other hand, antibacterial metal elements can be incorporated into implant surfaces to inhibit initial adhesion of bacteria and prevent post-surgery, thus enhancing the antibacterial property [34]. Furthermore, the content of bioactive elements and antibacterial metal elements on MAO coating surface can be tuned by controlling voltage, electrolyte components and MAO time[51]. To our best knowledge, this specific topic has not been reviewed in the recent literature. The aim of the review is to collect and compare the recent scientific papers concerning surface modification of Ti with the incorporation of antibacterial metal elements (*e.g.* Ag, Cu, Zn) to endow antibacterial properties by MAO. The review focuses mainly on the effects of the composition and concentration of electrolyte and process parameters (voltage, current density, oxidation time) on morphological characteristics, antibacterial ability and biocompatibility of MAO coating. MAO assisted by magnetron sputtering (MS) to achieve superior antibacterial property and biocompatibility is also discussed, following the forecast of the development trend of MAO in the future.

2. Micro-arc oxidation method

MAO, which is also referred to as plasma electrolyte oxidation (PEO), is a high voltage plasma-assisted anodic oxidation process. MAO is a relatively convenient technique for forming firmly adherent oxide ceramic layers on the surfaces of valve metals such as Ti, Al, Mg, Zr, Ta and their alloys. As showed in Fig.1, MAO process was controlled by a MAO power supply. Before MAO, the non-working side of specimen was connected with copper conductor and coated with acrylate adhesive. During the MAO process, the specimen was conducted as anode and the stainless steel electrolytic bath was regarded as cathode to fill with electrolyte. The stirrer was applied to keep the electrolyte uniform and the circulating water treatment system was used to sustain the temperature of electrolyte below 30℃.

The principle of MAO is explained in Fig.2. At the initial stage of MAO treatment, as soon as the specimen is exposed to the electrolyte, the voltage increases rapidly and linearly with time and an anodic barrier film, also called a passivating film (Fig.2a), is initially formed on the surface of specimen. Soon afterwards, with the increase of voltage, some tiny oxygen bubbles can be observed and a porous insulating oxide layer, which usually grows under conditions of dielectric breakdown, forms on the surface of specimen[52]. In this stage, the voltage and current flow follow the Faraday's law, which is corresponding to the conventional anodizing stage (Fig.2b). When the applied voltage on the specimen surpasses the dielectric breakdown of insulating oxide coating, dielectric breakdown takes place, leading to the formation of spark discharges (Fig.2c). The current flow only concentrates upon regions of breakdown, and the Ca, P elements from the electrolyte and the other elements from the specimen enter into regions of breakdown by diffusion and electrophoresis at intense local high temperatures, resulting in localized forming and thickening of the porous structure oxide coating. The discharge sparks gradually grow bigger and the micro-arcs discharges are transformed into powerful arcs discharge (Fig.2d). When the new generated oxide coating (Fig.2e) is capable of resisting current flow, the other regions are vulnerable to breakdown due to the smaller resistance and finally the chemical reaction interface would move towards the entire surface[53]. Breakdown of the coating occurs at a vulnerable spot of the growing oxide film. Meanwhile, the new porous structure oxide coating might also be formed and thickened by the emission of gas due to intense local high temperatures at the sites of breakdown[54]. As the prolonging of oxidation time, large discharge channels with intense sparking and gas bubbles would emerge at the surface, leading to the formation of larger protruding pores even spongy interconnected microstructure (Fig.2f). The continuous formation and breakdown of the oxide

Peer-reviewed version available at Coatings 2017, 7, 45; doi:10.3390/coatings7030045

coating (Fig.2g) causes the potential to fluctuate. Both the dissolution of base material and gasification of the electrolyte enable the formation of porous ceramic oxide coating (Fig.2h).

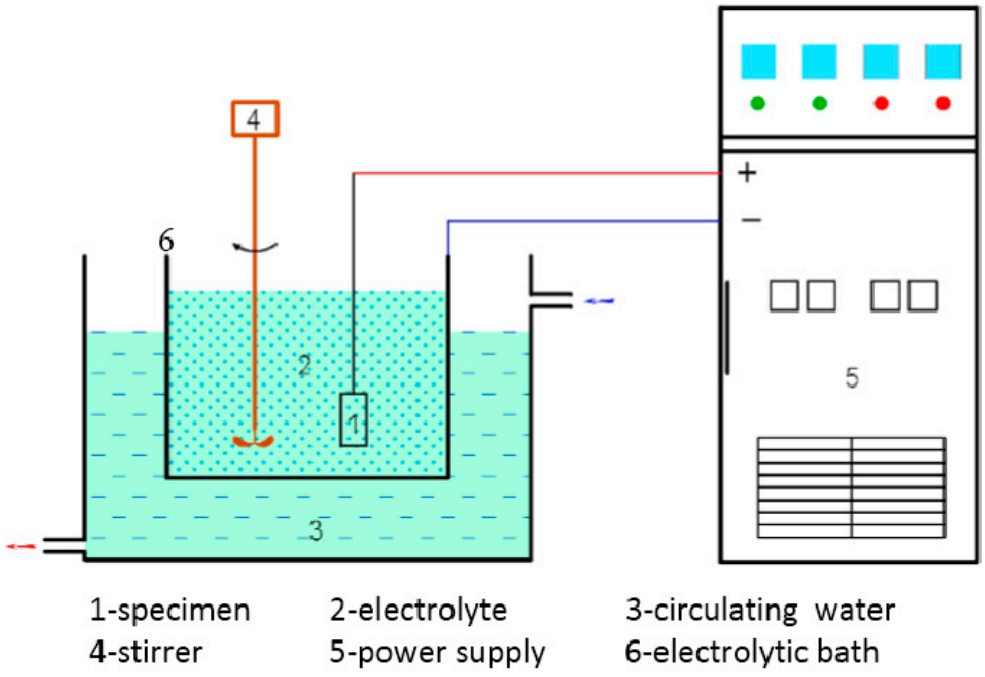

Fig.1 Schematic diagram of the MAO experimental device.

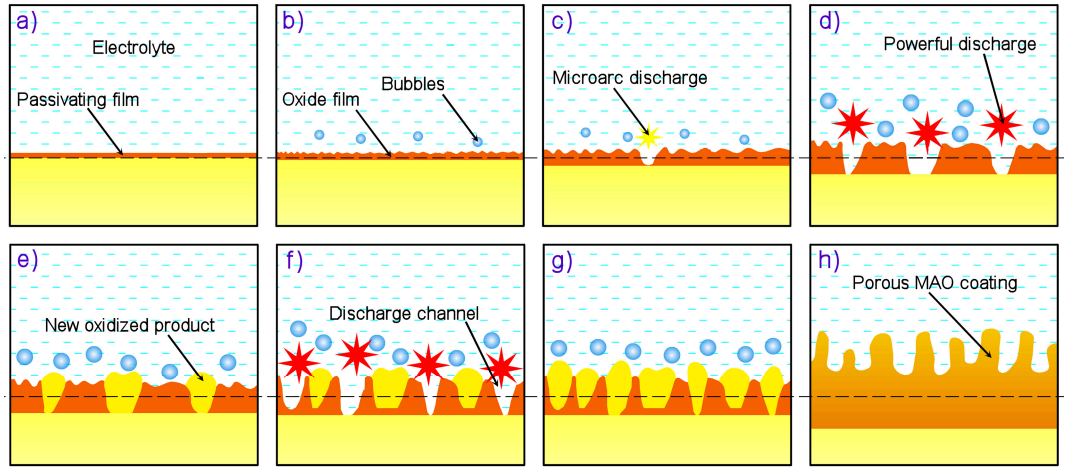

Fig.2 Schematic of the formation process of MAO porous coating.

The composition of the MAO electrolytes has a dramatical effect on the morphological characteristics, such as porosity and thickness of MAO coatings. Hence, the proper selection of the electrolyte composition is imperative to obtain the satisfactory performance. Generally, different antibacterial metal elements mixed with calcium acetate (CA) and glycerophosphate disodium (GP) are used as the base electrolyte in MAO process to enhance the antibacterial property of the implant materials. The characteristics of the fabricated antibacterial coating prepared by MAO techniques are briefly summarized in Table 1 and the details are reviewed according to the difference of doping way of antibacterial metal elements.

Table 1. Summary of the characteristics of antibacterial coating by MAO.

Ti alloy	Electrolyte	Electrical parameter			Surface topography (pore size)	XRD detected phase	Surface content of Ag/Cu/Zn (wt.%)	Release amount of Ag/Cu/Zn (ppb)	Tested bacteria	Biocomp-atibility	Refere-nces
		Voltage (V)	Current density ($A \cdot dm^{-2}$)	Oxidation time (s)							
Ti-6Al-7Nb	0.02 M Ca-GP, 0.15 M CA, and 3.0 $g \cdot L^{-1}$ Ag NPs	<250	20	300	Porous structures (<3μm) with Ag NP of 37nm	Ti, Rutile and Anatase	0.03	-	*S.aureus*	-	[55]
Ti-6Al-7Nb	0.02 M Ca-GP, 0.15 M CA, and 3.0 $g \cdot L^{-1}$ Ag NPs	<250	20	0~300	Porous structures (<5μm) with Ag NP of 7–25 nm	-	-	-	-	-	[56]
Ti-6Al-7Nb	0.02 M Ca-GP, 0.15 M CA, and 0.3 $g \cdot L^{-1}$ Ag NPs	234 ± 3	20	300	Porous structures (<5μm)	-	-	12	*S.aureus*	Human osteoblastic cell	[38]
Ti-6Al-7Nb	0.02 M Ca-GP, 0.15 M CA, and 3.0 $g \cdot L^{-1}$ Ag NPs	237 ± 2	20	300	Porous structures (<5μm)	-	-	89	*S.aureus*	Human osteoblastic cell	[38]
Cp-Ti	2 $g \cdot L^{-1}$ NaOH, 15$g \cdot L^{-1}$ NaH_2PO_4 and 3.0$g \cdot L^{-1}$ Cu NPs.	-	20	300	Porous structures (<5μm) with Cu NP of 60nm	-	-	-	*E.coli*, *S.aureus*	-	[57]
Cp-Ti	0.04 M β-GP, 0.4 M CA and 0.004 M $AgNO_3$	250~350	-	180	Spherical pores (<3μm)	Ti, Rutile, and Anatase	-	-	*S. aureus*	Human osteosarcoma	[58]

										(HOS) cell	
Cp-Ti	0.04 M β-GP, 0.4 M CA and 0.004 M $AgNO_3$	420	-	180	Irregular and rough pores with spherical particles and flake	Rutile, β-$Ca_2P_2O_7$, α-TCP, and HA	0.21–0.45	-	*S. aureus*	Human osteosarcoma (HOS) cell	[58]
Cp-Ti	0.04 M β-GP, 0.4 M CA and 0.00006 M $AgNO_3$	420	-	180	Irregular and rough pores with spherical particles and flake	Rutile, β-$Ca_2P_2O_7$, α-TCP, and HA	0.1	-	*S. aureus*	Human osteosarcoma (HOS) cell	[58]
Ti6Al4V	β-GP, CA and 0.1 g·L^{-1} $AgNO_3$	400	-	300	Granular morphology with Ag NPs of 20–30 nm	Ti, Rutile, Anatase, $CaTiO_3$ and HA	0.6	2500	*E. coli*	-	[59]
Ti6Al4V	β-GP, CA and 0.4 g·L^{-1} $AgNO_3$	400	-	300	Needle-like morphology with Ag NPs of 20–30 nm	Ti, Rutile, Anatase, $CaTiO_3$ and HA	2.1	8000	*E. coli*	-	[59]
Cp-Ti	Na_2HPO_4, CA, and 0.0025 M CH_3COOAg	380	-	300	Flake-like morphology with regional Ag particles less than 200 nm	Ti, Rutile, Anatase, $CaTiO_3$ and HA	4.6	-	*E.coli*, *S.aureus*	-	[60]
Cp-Ti	0.5~1.0 g·L^{-1} $AgNO_3$	-	65	5~240	Highly ordered	-	-	200~450	*S.aureus*	Newborn	[61]

					nanopores with Ag NPs of 10–30 nm within micropits					mouse pre-osteoblast cells	
Cp-Ti	7.6 g·L^{-1} Na_3PO_4, 9.4 g·L^{-1} $Ca(NO_3)_2$ and 1.0 g·L^{-1} $AgNO_3$	-	65	240	Highly ordered nanopores with Ag NPs of 10–30 nm within micropits	-	-	-	*S.aureus*	Newborn mouse pre-osteoblast cells	[61]
Cp-Ti	1.0~8.0 g·L^{-1} $Cu(NO_3)_2$	-	65	240	Mesopores (20-40 nm) within micropits	Ti	-	-	-	Osteoblast cells	[62]
Cp-Ti	3.8~7.6 g·L^{-1} Na_3PO_4 and 1.0 g·L^{-1} $Cu(NO_3)_2$	-	65	240	Mesopores (20-40 nm) within micropits	Ti	-	-	-	Osteoblast cells	[62]
Cp-Ti	0.05 M β-GP, 0.1 M CA and 0.05 M $(CH_3COO)_2Cu$	-	16.5	240	Micropores or crater structures (3-5 μm) with nano-grains of 30-50 nm	Ti and Anatase	1.43	-	*S.aureus*	Human osteosarcoma cell	[63]
Cp-Ti	0.02 M β-GP, 0.2 M CA and 0.00125~0.005 M Cu $(CH_3COO)_2$	450	-	90	Micropore structures (1-4μm)	Rutile and Anatase	0.67~1.93	2.8~60.2	*S.aureus*	Mouse fibroblast cell	[64]
Cp-Ti	0.15M Ca-GP, 0.02M CA and 0.06M ZA	-	30	300	Porous structures (<5μm)	Ti, Rutile and Anatase	8.7	-	*E.coli*, *S.aureus*	Osteoblast cells	[65]

Cp-Ti	0.05 M β-GP, 0.1 M CA and 0.02~0.06 ZA	-	16.5	240	Microporous structures (<5μm)	-	4.6~9.3	1000~3620	*E.coli*, *S.aureus*	Rat bone mesenchymal stem cells	[10]
Cp-Ti	0.02M β-GP, 0.1M CA, 0.1M ZA, and 6 g·L^{-1} Ag NPs	390	-	30~90	Microporous structures (1–4 μm)	Anatase and Rutile	1.06~1.42 (Ag), 22.19~26.93(Zn)	-	*S.aureus*	-	[66]
Cp-Ti	0.02M β-GP, 0.1M CA, 0.1M ZA, and 6 g·L^{-1} Ag NPs	390	-	120	Microporous structures (1–4 μm) with Ag NPs of 5–10 nm	Anatase, Rutile and ZnO	1.56(Ag), 29.38(Zn)	684(Ag), 6880(Zn)	*S.aureus*	-	[66]
Cp-Ti	0.02M β-GP, 0.1M CA, 0.1M ZA, and 6 g·L^{-1} Ag NPs	390	-	240	Microporous structures(1–4 μm) with some deposits	Anatase, Rutile, ZnO and Zn_2TiO_4	1.58(Ag), 31.27(Zn)	-	*S.aureus*	-	[66]

2.1. Introduction of metal nanoparticles into MAO electrolyte

NPs present a greater chemical activity than the bulk material for the advantage of their larger ratio of surface area to volume[67]. Ag NPs are the most popular inorganic antimicrobial NPs [68] and can be incorporated into implant by directly dispersion of solid Ag NPs in the electrolyte during MAO. The antibacterial mechanisms as reported are Ag NPs can directly interact with the microbial cells, leading to the increase of membrane permeability[69], the degradation of lipopolysaccharide molecules with the formation of pits and gaps in the bacterial membrane and the damage of bacterial outer membrane[70,71]. Ag NPs can also penetrate the bacterial cell envelope and cause DNA damage and protein oxidation by producing secondary products such as reactive oxygen species[72]. It has also been demonstrated that the antimicrobial activity of Ag NPs is higher than that of Ag ion[73]. The use of Ag NPs will lead to anti-bacterial effects maximized due to the increased numbers of particles per unit area[67].

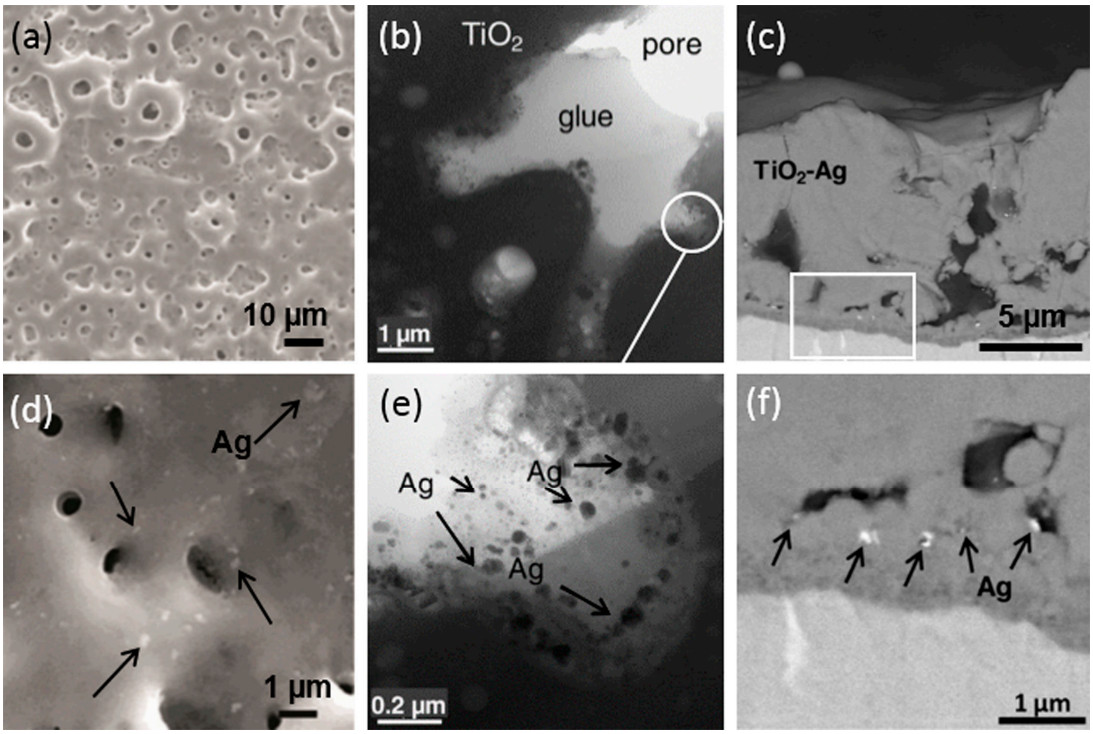

Fig.3 Low and high magnification surface SEM images(**a**, **d**), bright field TEM images (**b**, **e**) and cross-sectional SEM images(**c**, **f**) of the bactericidal coatings showed that the Ag NPs are distributed on the porous surface, in the micropores or embedded in the dense oxide layer [38,56].

Necula *et al.* [55] have successfully fabricated Ag-bearing TiO_2 coatings with different contents of Ag NPs by MAO in the electrolyte including CA, calcium glycerophosphate (Ca-GP) with Ag NPs. The morphology of metallic Ag NPs is similar to that of the particles in the electrolyte [56]. The average size of Ag NPs was measured to be 37 ± 6 nm. Under the assistance of electrophoresis during MAO, Ag NPs were homogeneously absorbed on the porous surface (Fig.3a and d)[38], transmitted to the inner pore walls of the titanium oxide along the short-circuit paths (Fig.3b and e) [55,56] or embedded in the dense oxide layer(Fig.3c and f)[56]. The incorporation of Ag NPs in the titanium dioxide (TiO_2) matrix has no effect on the surface morphology of the coatings. All the layers were porous with well-defined pore ranging in size from a few nanometers up to 5μm [38], which are the typical morphology of MAO. Moreover, the contents of Ag NPs on the surface gone up with increased amount of Ag NPs in the electrolyte. They found that Ag NPs displayed good antibacterial activity against methicillin-resistant *Staphylococcus aureus* (*S. aureus*), one of the most problematic pathogen for orthopaedic implants, while showed little cytotoxicity to human osteoblastic cell line with the adjustment of the content of Ag NPs on TiO_2/Ag coating by decreasing the concentration of

the Ag NPs in the electrolyte [74]. However, the coatings prepared by this method are expensive due to the high price of Ag NPs.

Cu can inactivate the central catabolic and biosynthetic pathways, namely catalytic clusters of dehydratases [75], which endows Cu with strong antibacterial properties. Yao *et al.*[57] have prepared Cu-doped TiO_2 coatings by MAO in the working electrolyte containing NaOH, NaH_2PO_4 and 3 $g \cdot L^{-1}$ Cu NPs. The results of top-surface morphologies revealed that Cu NPs distributed both on the Cu-doped coating surface and inside the pores (Fig.4a). The size of most of the NPs was less than 60 nm. High-resolution XPS spectra indicated that Cu mainly existed in the Cu^{2+} (from CuO) state (Fig.4b). Cu-doped TiO_2 coatings showed excellent antibacterial properties attributed to the incorporation of Cu NPs with a high surface area to volume ratio, which would directly kill bacteria and release copper ions. Similar mechanism was reported by Raffi *et al.* [76], in which the reason of antibacterial property of Cu NPs was mainly ascribed to the adhesion of Cu NPs onto bacteria surfaces, namely direct contact-killing, since Cu NPs are oppositely charged with bacteria. When they encounter, the reduction reaction will occur at the bacterial cell wall, resulting in the formation of cavities/pits. Though Usman *et al.* [77] have also testified the antimicrobial and antifungal activities of Cu-chitosan NPs against methicillin resistant *S. aureus*, *B. subtilis*, *C. albicans*, *P. aeruginosa* and *Salmonella choleraesuis*, Pape *et al.* [78] have confirmed that the antibacterial activity of Cu NPs was significantly weaker than that of Ag NPs. Moreover, Cu NPs were rapidly oxidized when exposed to air[79], limiting their application.

With the consideration of the bad dispersion of NPs in solution and the weak adhesion of NPs onto the coating surface, only the several valuable studies have been documented in the field of antibacterial NPs by MAO so far.

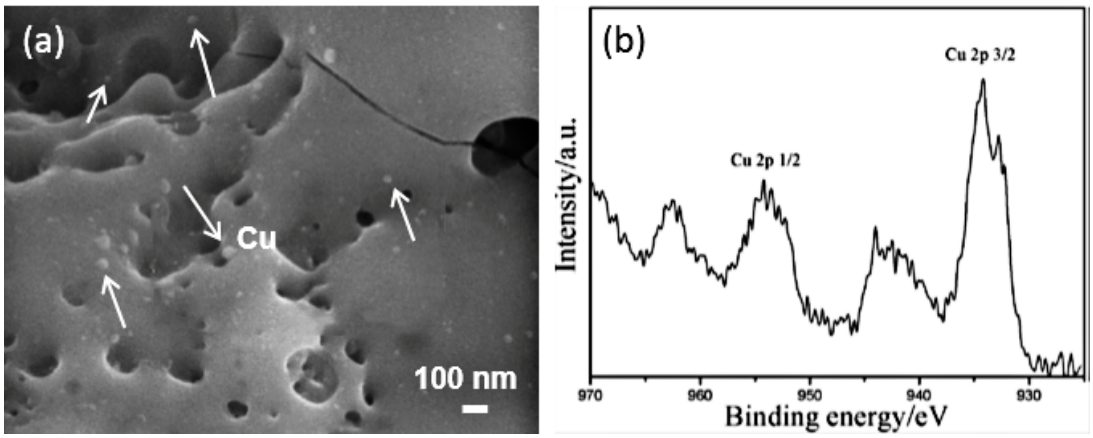

Fig.4 SEM micrographs of Cu-doped coatings revealing the presence of Cu nanoparticles on the surface and inside the pores (**a**). High-resolution XPS spectra of Cu 2p in TiO_2 coating indicated that Cu mainly exists in the CuO state (**b**) [57].

2.2. Introduction of metallic compounds into MAO electrolyte

For the biomedical industry, it seems to be an attractive strategy to endow implants surface with metallic coatings. Recent studies [45,80,81] have shown that biological or antibacterial elements can be incorporated into the coating during MAO process by introduction of metallic compound into MAO electrolyte. Ag-containing coatings have occupied the largest share of the global antibacterial market.

Song *et al.*[58] have incorporated Ag into Ti implants by MAO in 0.04 M β-glycerophosphate disodium salt pentahydrate (β-GP), 0.4 M CA and silver nitrate ($AgNO_3$) or silver acetate (CH_3COOAg) electrolytic solution at a fixed applied voltages range from 250V to 450 V. The addition of $AgNO_3$ reduced the required voltage for the formation of calcium phosphate compounds from 450V to 400 V [82,83]. When the concentration of $AgNO_3$ was fixed at 0.004 M, the oxidized layers was porous microstructure with spherical pores at the voltages below 350V (Fig.5a), while the

Peer-reviewed version available at Coatings 2017, 7, 45; doi:10.3390/coatings7030045

coating surface became rough and covered with spherical particles and flakes above 380V (Fig.5b) due to the existence of calcium phosphate compounds (Fig.5c). MAO coatings containing 0.21–0.45 wt.% of Ag were cytotoxic to human osteosarcoma MG63 cells, while Chen *et al.* [84] reported that 2.05 wt % Ag displayed no osteoblast cytotoxicity. The comparison results indicated that the cell proliferation not only has relation to the content of Ag, but also depends on other factors such as surface roughness of the coatings[85]. The relatively smooth coating oxidized at 400 V with lower content of Ag (0.00006 M $AgNO_3$) exhibited no cytotoxicity with the unreduced antibacterial property.

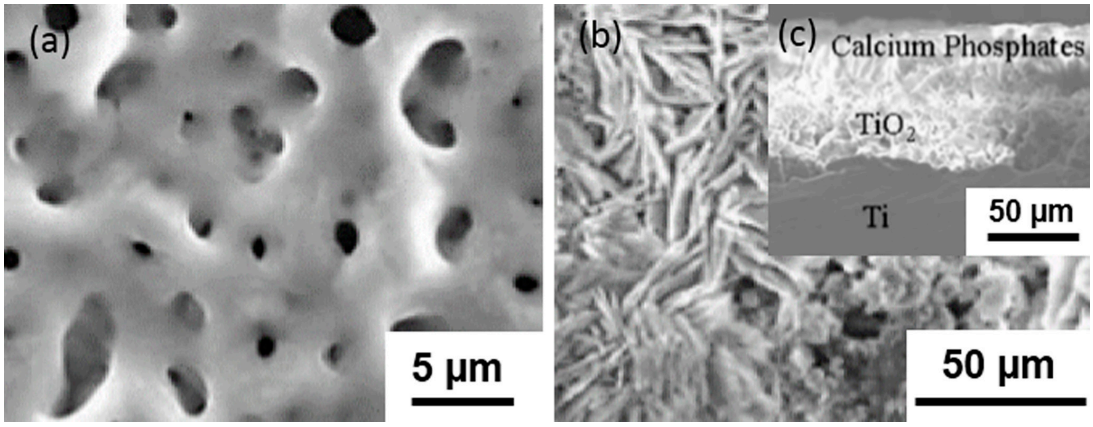

Fig.5 Surface morphologies of MAO samples obtained in electrolyte solution containing 0.004 M AgNO3 for 3 min at 350 V (a) and 400 V (b). (c)The cross section view of specimen (b) [59].

Muhaffel *et al.*[59] have also prepared the novel multi-layer coatings composed mainly of inner TiO_2 layers and outer HA layers via MAO in β-GP and CA electrolyte with different addition level of $AgNO_3$ (0.1 $g{\cdot}L^{-1}$ and 0.4 $g{\cdot}L^{-1}$). Unlike the general surface characteristics of MAO coatings, micro-pores were hardly identified owing to the existence of outer granular HA on MAO-0 (Fig.6a), MAO-0.1 (Fig.6b) or needle-like HA layers on MAO-0.4 (Fig.6c). Addition of $AgNO_3$ can speed up MAO process at higher current density levels and enhance the crystallinity of the HA layer and precipitation of Ag NPs on the HA layer. Compared to amorphous HA, the crystalline HA exhibits better bioactivity in SBF and biointegration [86]. Ag NPs with the size of 20–30 nm were deposited on the HA layer of MAO-0.1 (Fig.6e) and MAO-0.4 (Fig.6f). The rapid release of Ag^+ ions at the initial periods and the subsequent slower release contributed to long-term antibacterial activity. Moreover, cumulative release of Ag^+ ions (2.5ppm for MAO-0.1 and 8ppm for MAO-0.4) was lower than the toxic concentration (10 ppm) of Ag for human cells[87]. Overall consideration, 0.1 $g{\cdot}L^{-1}$ $AgNO_3$ appeared exhibited sufficient antibacterial activity and no risk of cytotoxicity while preserving the structural characteristics. Muhaffel *et al.*[60] have further reported the multi-layer coating consisting of subnatant TiO_2 layers and upper bio-mimetic precipitation in disodium hydrogen phosphate(Na_2HPO_4), CA, and 0.0025 M CH_3COOAg electrolyte at 380V. Incorporation of 4.6wt.% Ag into the multi-layer led to superior antibacterial efficiency against *Escherichia.coli* (*E. coli*) and *S. aureus* while conserving the biomimetic apatite precipitation. The multilayer consisted of three layers: a thin compact TiO_2 layer above the substrate showing better substrate bonding, a middle layer of a porous and thick TiO_2 layer on the compact layer, and a flake-like top layer of biocompatible compound layer incorporated with regional Ag particles (Fig.7).

Peer-reviewed version available at Coatings 2017, 7, 45; doi:10.3390/coatings7030045

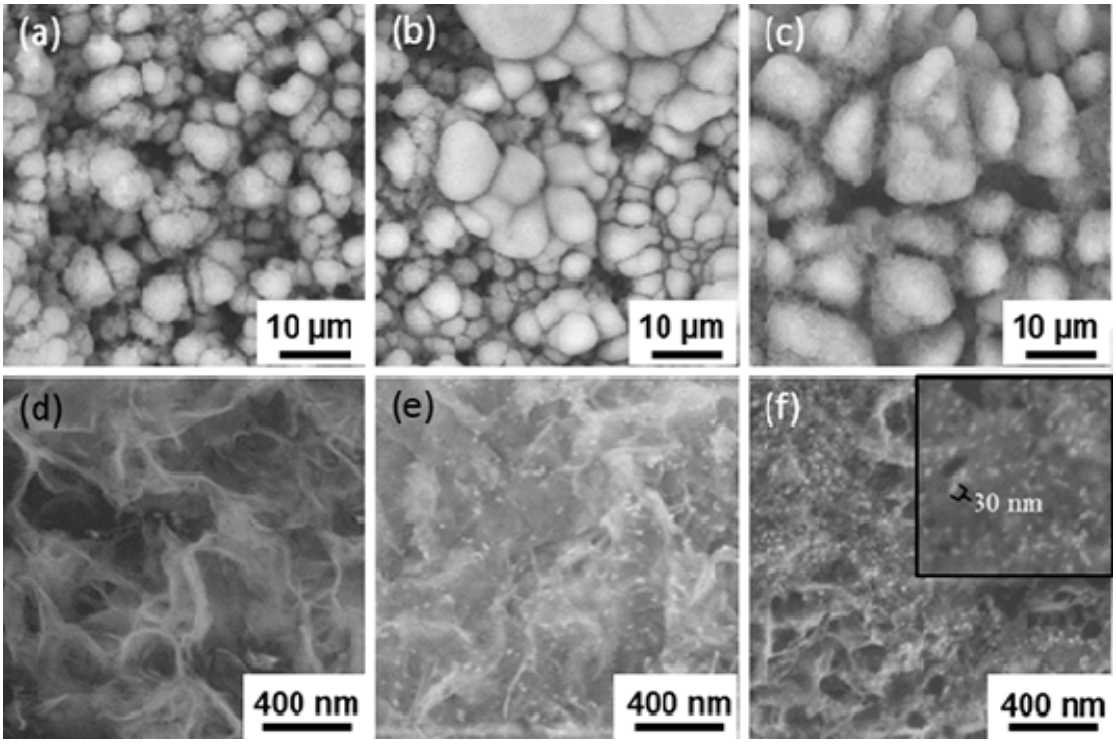

Fig.6 Low and high magnification SEM micrographs of MAO-0(**a, d**), MAO-0.1 (**b, e**) and MAO-0.4 (**c, f**) [59].

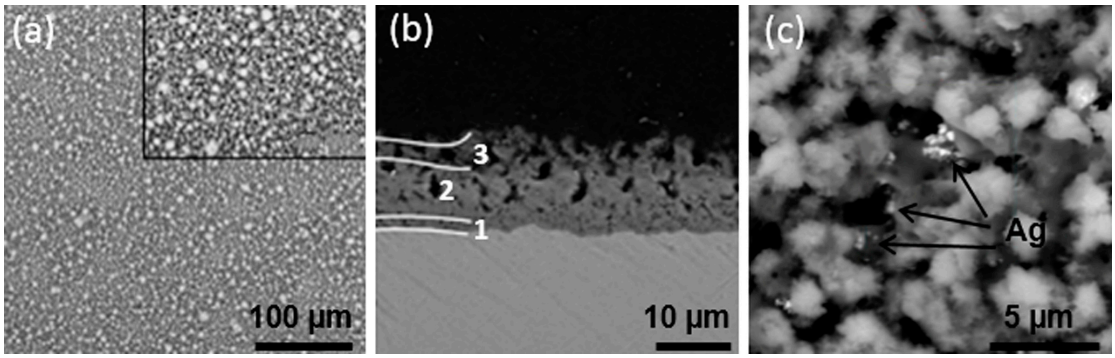

Fig.7 Low magnification surface(**a**) and Cross-sectional SEM (**b**) micrographs for the MAO-Ag samples obtained in electrolyte solution containing 0.0025 M CH_3COOAg (1: compact TiO_2 layer, 2: porous TiO_2 layer, 3: biocompatible compound containing layer)**. (c)** High magnification surface SEM micrographs indicated that regional Ag particles covered the surface [60].

Unlike the common surface micrometer-sized pores of MAO coatings, highly ordered nanopores (Fig.8b and c) within micropits (Fig.8a) were successfully prepared by Chang *et al.*[61] via a novel one-step high-current anodization (HCA) at the current density of 65 $A{\cdot}dm^{-2}$ in $AgNO_3$ electrolyte range from 0.5 to 16 $g{\cdot}L^{-1}$. The nanopore diameter decreased and the wall thickness increased with increasing of $AgNO_3$ concentrations (Fig.8d). Due to the controllable dimensions, the nanoporous structure modulated osteoblast functions, accommodating various clinical needs [88-90]. Scratch tests showed significantly enhanced bonding strength on the HCA treated sample (Fig.8e) in comparison with flaking on the anodized sample (Fig.8f) even at a small normal load. The TEM and XRD showed that Ag was embedded in crystallized TiO_2 in the form of crystallized AgO NPs with diameters between 10 nm and 30 nm. The crystallized TiO_2 also contributed to good bioactivity[49]. Gao *et al.* [91] reported that several ppb of Ag release quantity were capable of killing all the bacteria. So the high release level of Ag (>200ppb) revealed strong antimicrobial properties, but resulted in severe cytotoxicity. To improve the cytocompatibility and reduce toxicity, Na_3PO_4

Preprints (www.preprints.org) | NOT PEER-REVIEWED | Posted: 14 March 2017 doi:10.20944/preprints201703.0072.v1

Peer-reviewed version available at Coatings 2017, 7, 45; doi:10.3390/coatings7030045

and $Ca(NO_3)_2$ were added into the electrolyte to inhibit the formation of nanopores to a certain extent and to lower the release of Ag^+ while preserving their antibacterial ability.

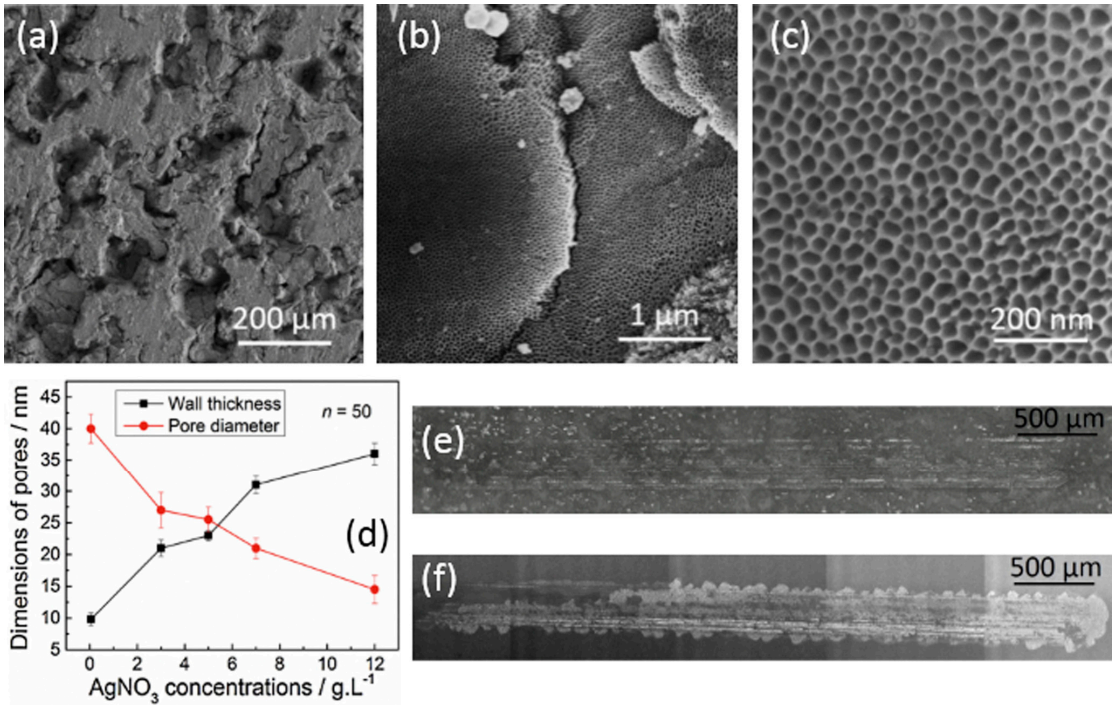

Fig.8 Low-magnification (**a**) and high-magnification (**b, c**) SEM images of the high-current anodization (HCA) treated sample in $AgNO_3$ electrolyte. (**d**) Variation of the pore diameters and thickness of the HCA treated samples as a function of $AgNO_3$. Scratch SEM images of sample anodized in the electrolyte with the $AgNO_3$ concentration of 2 $g{\cdot}L^{-1}$ (**e**) and sample anodized in ethylene glycol supplemented with 0.5 wt% NH_4F, 5.0 vol% H_2O, and 5.0 vol% CH_3OH at an applied voltage of 30 V for 1.5 h at room temperature (**f**) showed the significantly enhanced bonding strength on the HCA treated sample [61].

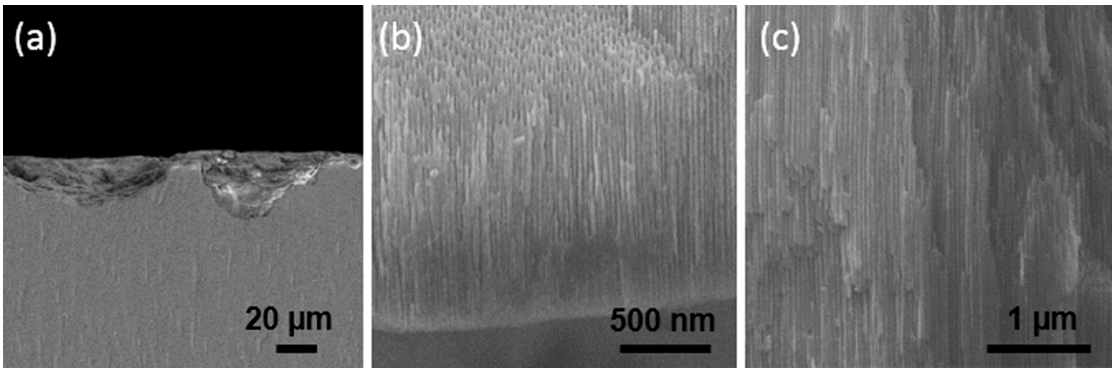

Fig.9 Low (a) and high magnification (b, c) cross-sectional SEM images of the high-current anodization (HCA) treated sample in $Cu(NO_3)_2$ electrolyte indicated the presence of highly-ordered nano-channels [73].

Likewise, the unique structure with micro/nano-morphology can also be obtained in $Cu(NO_3)_2$ electrolyte due to field-assistant chemical etching of NO_3^-. Huang *et al.*[62] believed that use of $Cu(NO_3)_2$ instead of $AgNO_3$ as electrolyte may avoid the potential cytotoxity of heavy metal ions. Ag^+ was easily oxidized to higher valence (Ag^{2+}), which will lead to severe cytotoxicity[61]. However, bivalent Cu^{2+} in $Cu(NO_3)_2$ cannot be further oxidized. The results of EDX and XPS confirmed that toxic elements Cu was exactly not incorporated into the coating surface, so copper

will not directly contact with cells to produce cell toxic. Cross-sectional images (Fig.9) also indicated that highly-ordered nano-channels were perpendicular to the substrate, and a compact layer can be observed between the nanopore arrays and the substrate. Besides, the addition of PO_4^{3-} in the electrolyte further improved the cellular performance[92,93]. Moreover, A well-defined micro/nano-morphology can also be acquired by this HCA technique in electrolyte such as $Cu(NO_3)_2$, $Zn(NO_3)_2$, (Na_3PO_4 + $Ca(NO_3)_2$ + Na_2SiO_3), and (Na_3PO_4 + $AgNO_3$ + Na_2SiO_3), which will extend its application.

As an essential trace element for living organisms, Cu participates in a variety of metabolic activity, so it might be more suitable for antibacterial application compared to Ag. Zhu *et al.* [63] prepared porous and nano-structured Cu-incorporated TiO_2 coatings by MAO in a novel Cu-containing electrolyte containing 0.05 M β-GP, 0.1 M CA and 0.05 M copper acetate($Cu(CH_3COO)_2$) at 16.5 $A{\cdot}dm^{-2}$ for 4 min. The result showed that Cu-TiO_2 coatings displayed rough micropores or crater structures with the diameter of 3-5 μm (Fig.10a), and the coatings were fully covered with nano-grains with the size of 30-50 nm (Fig.10b) at a higher magnification. The antimicrobial activity of Cu-TiO_2 coatings was improved due to the inhibitory effect of Cu. Meanwhile, the osteoblastic adhesion, spreading, early proliferation and late differentiation on Cu-TiO_2 coatings were significantly enhanced due to the existence of the porous nano-structured surface produced during MAO, just like those found by other researchers[81,94]. Besides, Cu element also plays a vital role in various cell behavior, including osteoblasts[95], endothelial cells[96], bone marrow stem cells[63] and fibroblasts[64].

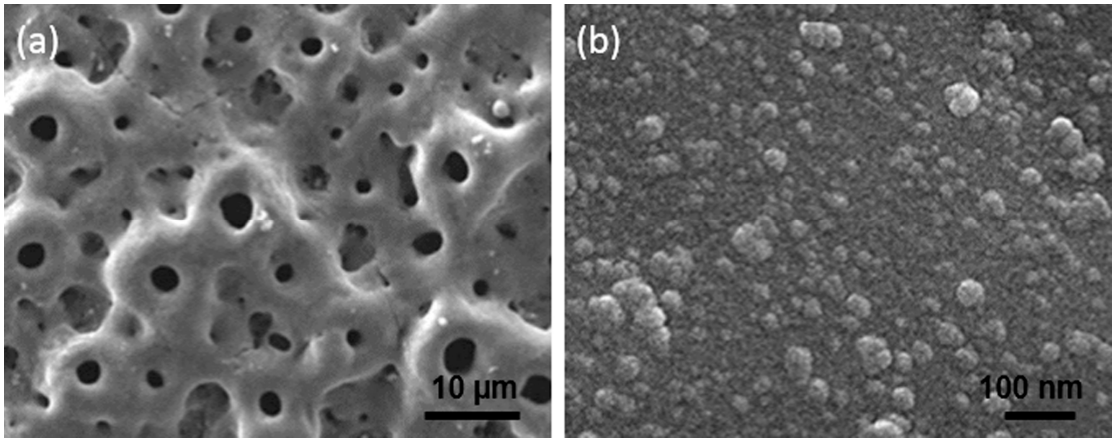

Fig.10 Surface morphologies of Cu-TiO_2 (**a**) and (**b**) coatings at different magnifications showing micropores with the diameter of 3-5 μm and nano-grains with the size of 30-50 nm on the surface of Cu-TiO_2 [63].

Zhang *et al.* [64] have investigated the tolerable and safe upper intake level of Cu^{2+} in order to improve the response of fibroblasts while maintaining the antibacterial activity. TiO_2 coatings doped with different amounts of Cu^{2+} were directly fabricated via MAO in copper acetate 0.02 M β-GP, 0.2 M CA and various amounts of $Cu(CH_3COO)_2$ (0.00125 M, 0.0025 M, 0.00375 M and 0.005 M). As shown in Fig.11a, the coatings still maintained the typical porous structure of MAO, and Cu content on the surface of the sample increased with the increase of the concentration of $Cu(CH_3COO)_2$ in electrolyte. Cu content also increased gradually from the substrate to the coating surface, and the apparent continuity between the coatings and Ti substrates indicated the strong bonding forces (Fig. 11b). As the dose of Cu^{2+} was increased, the number of adhering bacteria (Fig.11c) was obviously reduced due to the contact-killing and release-killing mechanism, and the bacterial morphologies and membrane integrities were subject to serious disruption (Fig.11d). Results of biological compatibility experiments showed that the appropriate dose of Cu (0.67 wt%, Cu1) can improve the adhesion and proliferation of fibroblasts and significantly support denser collagen deposition, while excess Cu^{2+} were poisonous to the cells(Fig.11e), and will disrupt fundamental cellular processes and trigger apoptosis, just as mesenchymal stem cells[97]. Cu1 prepared in 0.00125 M $Cu(CH_3COO)_2$

Preprints (www.preprints.org) | NOT PEER-REVIEWED | Posted: 14 March 2017 doi:10.20944/preprints201703.0072.v1

Peer-reviewed version available at Coatings 2017, 7, 45; doi:10.3390/coatings7030045

electrolyte with Cu mass fraction of 0.67 delivered the best compromise between antibacterial effectiveness and cytotoxicity.

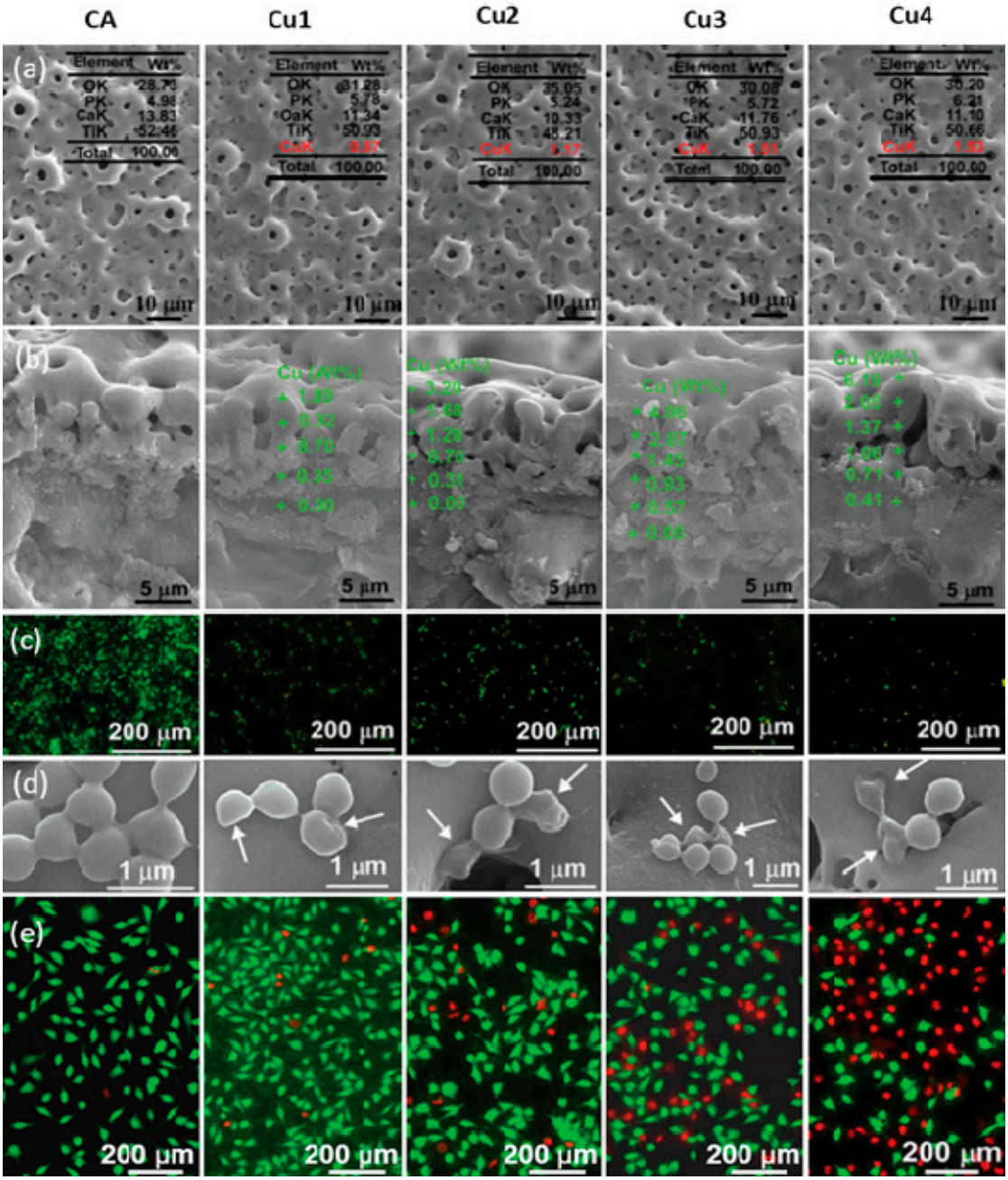

Fig.11 Surface (**a**) and cross-sectional (**b**) SEM morphologies images of the CA, Cu1, Cu2, Cu3 and Cu4 coatings showed that Cu content increases with the increasing concentration of $Cu(CH_3COO)_2$ in electrolyte. Live–dead assay (**c**), the corresponding bacterial morphologies (**d**) of *S. aureus* after 24 h of incubation and cell viabilities (**e**) of the cells cultured for 3 days are highly dependent on the amount of Cu content incorporated [64].

As one of the most important trace elements in human body, Zn also has been recognized recently[98], although the antibacterial activity of Zn is relatively weaker than that of Ag and Cu. For example, both Zhang *et al.*[65] and Hu *et al.* [10] used zinc acetate (ZA) solution to modify a titanium surface by MAO. Zhang *et al.*[65] prepared Zn-incorporated TiO_2 coatings in 0.06M ZA, 0.02M CA and 0.15M Ca-GP solution at a current density of 30 $A{\cdot}dm^{-2}$ for 5mins. Hu *et al.*[10] obtained Zn-incorporated TiO_2 coatings with different Zn contents (Z0 Z2 Z4 Z6) in mixtures solutions of different concentrations (0M, 0.02M, 0.04M, 0.06M) of ZA, 0.1 M CA and 0.05 M β-GP at 16.5 $A{\cdot}dm^{-2}$

for 4mins. It has been found that the incorporation of Zn in TiO_2 did not apparently change the surface topography, all the TiO_2 coatings were still typical porous surface morphology and the micropores with a pore size less than 5μm were uniformly distributed on the coating surface (Fig.12a). The coatings were primarily composed of anatase and rutile phase. Increasing the content of ZA in the electrolyte led to a slight increase in Zn content of oxide layer. However, the feature peaks of Zn-containing compounds were not detected due to the low concentration of Zn (4.6-9.3wt.%).The XPS showed that Zn existed in the form of ZnO (Fig.12b). The antibacterial mechanism of ZnO was attributed to the generation of reactive oxygen species(ROS)[99] on coating surface with higher Zn content(Fig.12c), rather than the low zinc ions release(<3.62 ppm)[100]. The accumulated released Zn ions not only facilitated the initial adhesion (Fig.12d), spreading and proliferation of bone marrow stem cells (bMSC)[98,101], but also up-regulated the gene and protein expression of bMSC while producing no cytotoxicity.

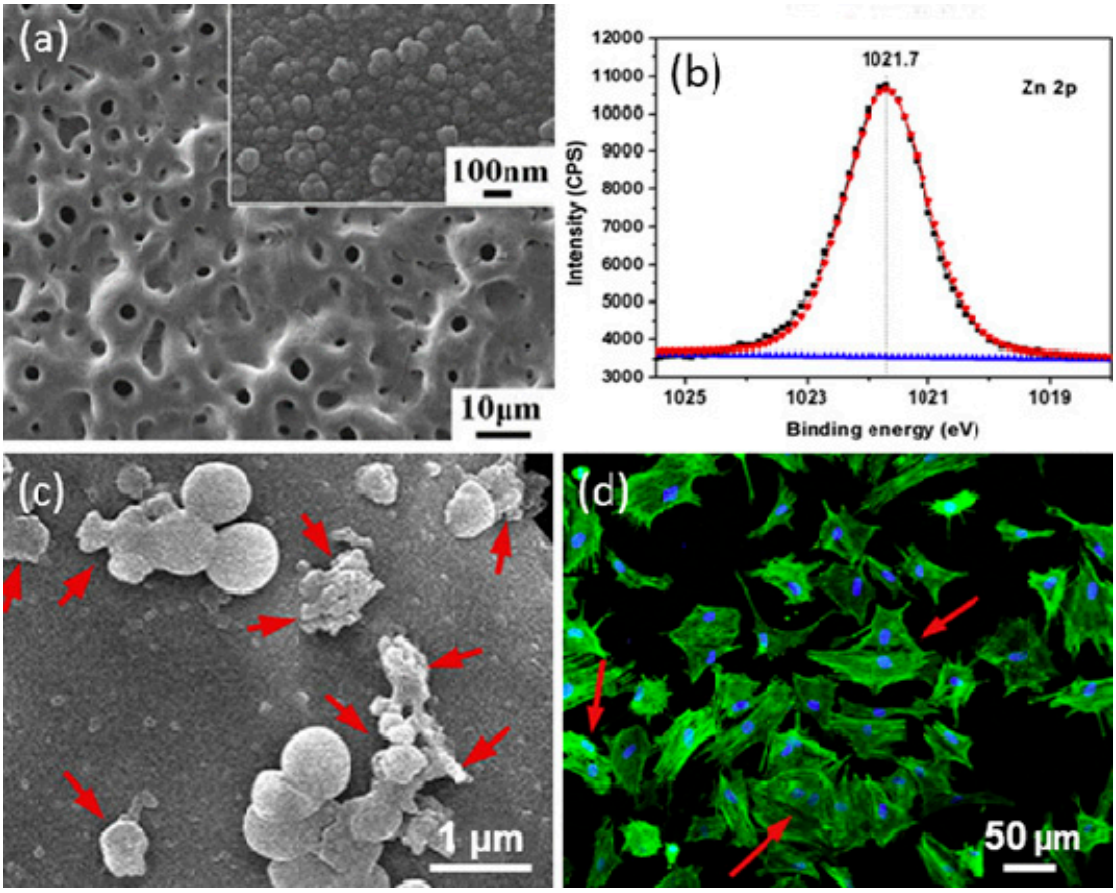

Fig.12 Surface SEM morphologies of Z6 coatings samples obtained in electrolyte solution containing 0.06 M ZA（zinc acetate） (**a**). High-resolution XPS spectra of Zn 2p in Z6 coating indicated that Zn mainly exists in the ZnO state (**b**). The obvious bacterial cell debris and completely lysed cells (indicated by red arrows) showed the improved antimicrobial property of Z6 coatings surfaces (**c**). The initial adhesion and spreading activity of bMSC cells after 24 h incubation on Z6 coatings were verified by the extraordinarily stretched cells morphology structure (**d**) and the presence of mitosis phase cells (indicated by red arrows) [10].

2.3. Introduction of both metal nanoparticles and metallic compound into MAO electrolyte

Recently, it has found that Zn^{2+} co-doped with small amount of Ag^{+} may lead to obvious increase of the antibacterial ability [102] in comparison with single Zn^{2+}. Zhang *et al.*[66] fabricated micro-porous TiO_2 coatings co-doped with Zn^{2+} and Ag NPs by MAO in the electrolyte composed of 0.1M CA, 0.1M ZA, 0.02M β-GP, 6 $g{\cdot}L^{-1}$ Ag NPs and 0.25 $g{\cdot}L^{-1}$ sodium dodecyl benzene sulfonate for 0.5, 1.5, 2 and 4 min. All the coatings were micro-porous with pore diameters of 1-4 μm (Fig.13a), but

Peer-reviewed version available at Coatings 2017, 7, 45; doi:10.3390/coatings7030045

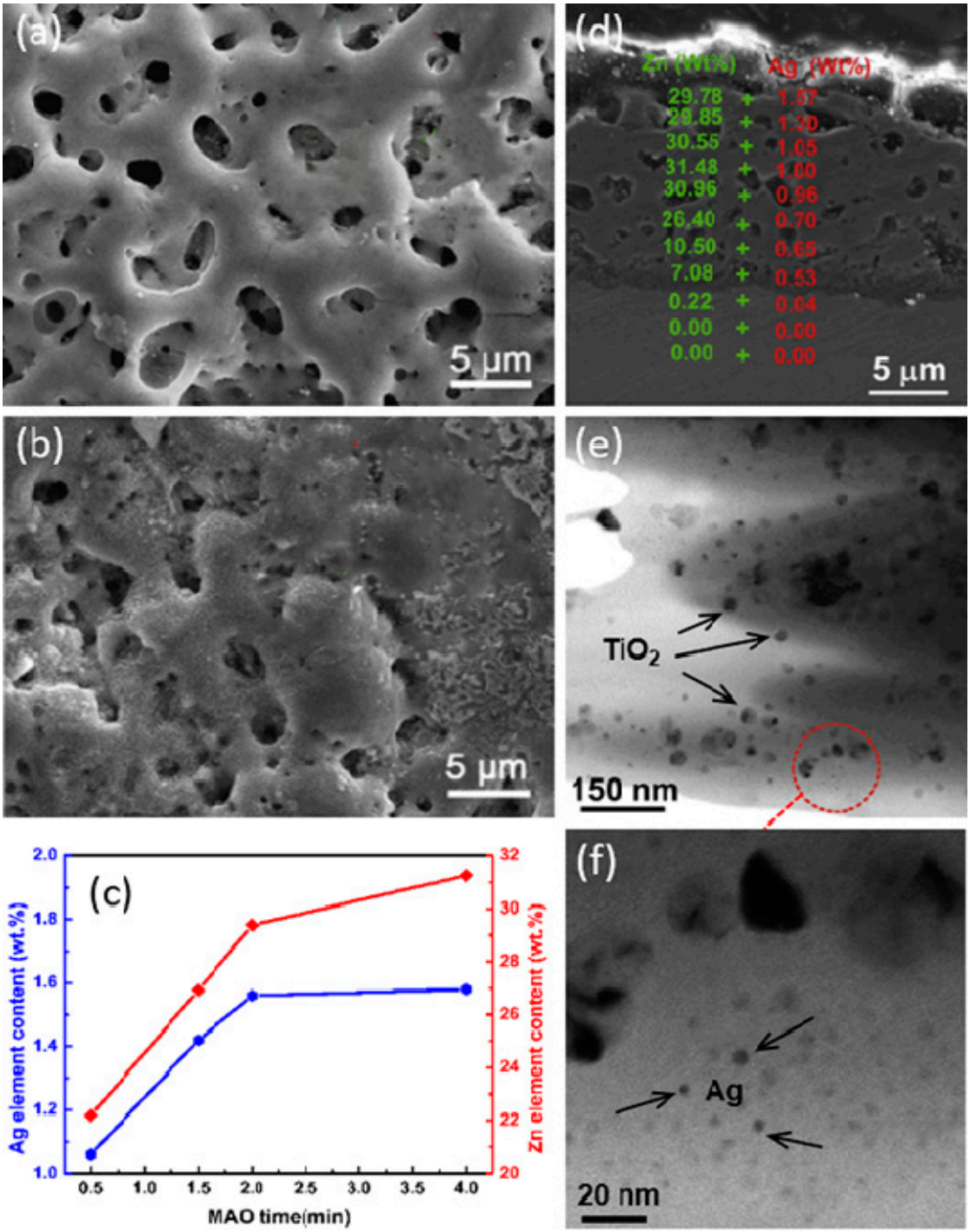

Fig.13 MAO treated coatings at 2 min (**a**) and 4 min (**b**) showed different surface morphologies in electrolyte solution containing 0.1M ZA, 6 g·L^{-1} Ag NPs. Cross-sectional morphology of the 2 min coating showed that the contents of Ag and Zn on the coating surfaces increased with prolonged MAO time (**c**) and increased gradually from the substrate to the coating surface (**d**). Low (**e**) and high (**f**) magnification TEM images showed the TiO_2 grains of 20-40 nm in size and nano-grains with the size of 5-10 nm [66].

some deposits displayed on micro-pores at 4 min (Fig.13b). The contents of Ag and Zn on the coating surfaces increased with prolonged MAO time (Fig.13c). Continuity between coating and substrate indicated strong bonding force by MAO, and the Ag and Zn contents increased gradually from the substrate to the coating surface (Fig.13d). Ag was composed of 73% Ag_2O and 27% metallic Ag[103,104], while Zn existed in the form of ZnO[105]. TEM images indicated that many large rutile or anatase grains of 20–40 nm in size (Fig.13e and f) and a lot of relatively small Ag nano-grains with

sizes of 5–10 nm (Fig.13f) were homogenously embedded in amorphous TiO_2 matrix. However, the diffraction spots of ZnO with trace amounts were not detected. The cumulative ion releases of Zn^{2+} (6.88 ppm) [10] and Ag^{+} (0.684 ppm) played an important role in inhibiting the growth of bacteria. Besides, the secondary products such as reactive oxygen species produced by Zn^{2+} and Ag^{+} were also harmful to bacteria. Carvalho *et al.* [106] and Jin *et al.* [28] have also proved the enhanced antibacterial activities of simultaneous incorporation of Zn and Ag into Ti. Jin *et al.* [28] believed that the interactions between Zn ions and bacteria were long-range based on the release of Zn ions[27], while the interactions between embedded Ag NPs and bacteria were short-range via the micro-galvanic effects without release of Ag ions[37,107]. Moreover, an appropriate amount of released Zn^{2+} also accelerated the osteogenic activity of rat bone mesenchymal stem cells (rBMSCs) via the long-range interactions.

2.4. MAO assisted by MS

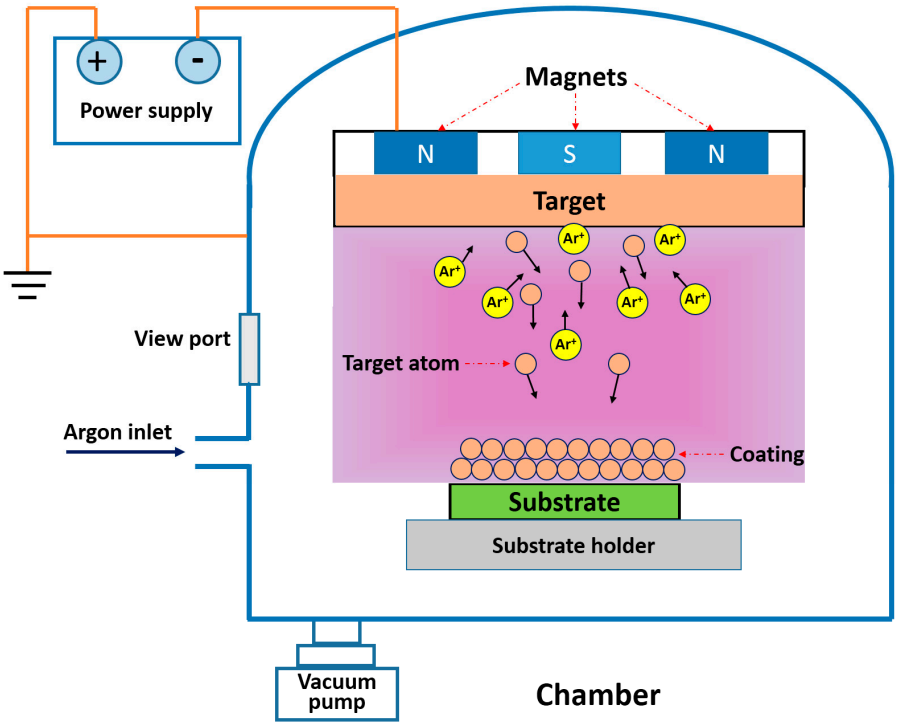

Fig.14 The schematic of the magnetron sputtering (MS) system.

MS magnetron sputtering (MS) is a deposition technique belonging to sputtering processes and is one of the physical vapor deposition (PVD) technologies. MS deposition process is conducted in inert gas (usually high-purity argon (Ar) gas) atmosphere regulated by the flow meter in a vacuum chamber. The specimens were placed in the sputtering chamber and high-purity Ar(99.999%) are introduced when the chamber sputtering is evacuated to a base pressure below 6×10^{-3} Pa. Films are deposited at various sputtering parameters such as gas flow, working pressure, sputtering power and sputtering time in order to acquire the desired properties of the material. For the sputtering process, there exists an electric field between the target material and the substrates. Under the action of electric field, Ar is ionized and bombards the target material located in the cathode of the discharge, which often cause the ejection of ions or atoms from the surface of target material toward that of the substrates. However, the lower ionization and bombardment rates of Ar often lead to the slower deposition rates and lower film densities. Given this, MS technology is introduced by installing a set of magnets beneath the target. The schematic of MS deposition system has been described in Fig.14. The magnets are used to provide a magnetic field to capture the secondary electrons emitted by the target. Under the action of magnetic field, secondary electron are bound in the high density plasma region near the target surface, do circular motion around the target surface

and constantly impact ionized large amounts of argon ion in the process of movement, thus improving the intensity of Ar ion bombardment and the deposition rate of the films.

MS is also an effective technique to incorporate antibacterial agents into the implant materials. The desired antibacterial ability can be obtained only by the choice of the optimal processing parameters. Bai *et al.*[108] have fabricated Ti-Ag composite coatings with different Ag contents (1.2 to 21.6 at.%) using co-sputtering Ti-Ag targets by MS. The composite coating showed long-term antibacterial ability. However, only the Ag on the surface of Ti-Ag composite coatings contributed to the antibacterial activity[109]. It is hence necessary to carry on a post-treatment to fully use the Ag on Ti-Ag composite coatings while the antibacterial activity is preserved.

By MS, The deposited AgTi layers cover the entire surface and are firmly combined with the substrate. The concentration of Ag in the layers can be accurately controlled only by adjusting the technological parameters. Though Ag will be dissolved into the electrolyte during MAO process, a great quantity of Ag still reserve in the MAO coating. MAO coating shows dense inner layer and rough porous outer structure. The dense inner layer can improve the mechanical interlocking ability and prevent the corrosion from body fluid, while the porous outer structure may increase the surface roughness thus promoting cell reaction. The desirable antibacterial ability and compatibility can achieve balance by this duplex technique of combining MS and MAO.

Zhang *et al.* [110] have developed the novel duplex-treatment technique combining MS with MAO to prepare the Ag-containing bioactive antibacterial coatings. AgTi layers were first deposited onto Ti by MS, then subjected to MAO at 20 $A \cdot dm^{-2}$ for 2, 5, and 8 min in the electrolyte containing 26.4 $g \cdot L^{-1}$ CA and 4.3 $g \cdot L^{-1}$ β-GP. The presence of Ag did not exert a significant influence on the voltage and surface morphology. Micron-sized pores were still distributed over the surfaces and pore sizes tend to increase (Fig.15a, b and c) due to the generated larger breakdown channels and more intense sparking with the increase of oxidation time. The coatings were comprised of rutile, anatase and a little Ag. However, Ag was uniformly distributed throughout the coating surface (Fig.15d), but in the form of Ag NPs [56]. During MAO, large amount of Ag was dissolved into the electrolyte, which caused a sharp decrease in Ag content of the MAO coatings. Ag, existing as metallic Ag^0 state, also showed excellent antibacterial ability.

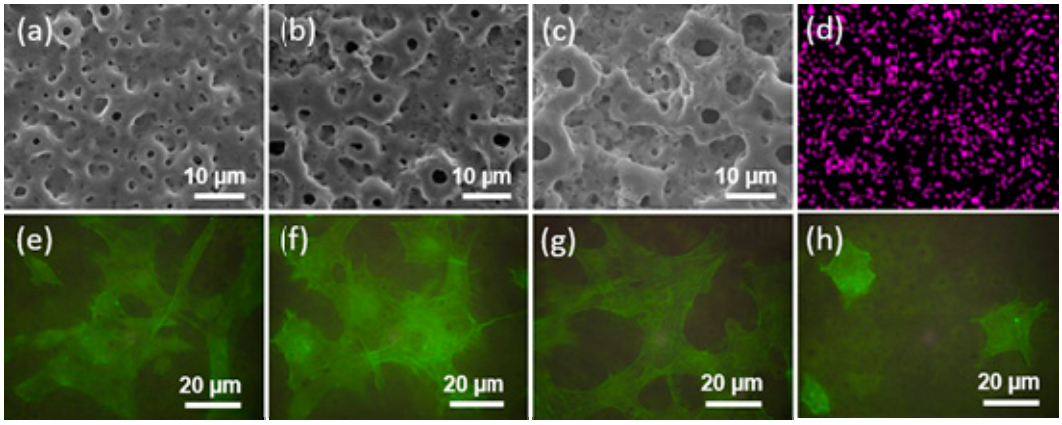

Fig.15 SEM surface micrographs of M-AgTi coating oxidation for 2 min (**a**), 5 min (**b**) and 8 min (**c**) indicated that the pore size increase with the increasing oxidation time. EDX maps showed Ag were uniformly distributed throughout the coating surface (**d**). Fluorescence microscopy images of F-actin cytoskeleton of pre-osteoblast cells cultured for 48 h on M0(**e**), M1(**f**), M2(**g**) and M3(**h**) coatings indicated that high concentration of Ag exhibited cytotoxic effect [110,111].

Furthermore, Zhang *et al.*[111] produced TiO_2 coatings with different Ag concentrations (M0, M1, M2, M3) by the above duplex-treatment technique. The concentration of Ag in the TiO_2 coatings increased with the increase of Ag incorporated in the AgTi layers. The initially high level and subsequently low level of Ag release provided relatively long-term antibacterial activities and met the clinical requirements. Nonetheless, M2 and M3 with 1.36 and 1.93 wt.% (Fig.15g and h) Ag

Peer-reviewed version available at Coatings 2017, 7, 45; doi:10.3390/coatings7030045

exhibited cytotoxic effect, which restricted cell proliferation and caused cell death. M0 with 0.95 wt.% Ag (Fig.15f) achieved the balance between antibacterial properties and good pre-osteoblast cell viability.

On this basis, He *et al.*[112] fabricated porous Ag/Sr-containing TiO_2 coatings via the similar method in the MAO electrolyte containing 0.167 M CA, 0.02 M β-GP and 0.033 M strontium acetate hemihydrate (SA). The coating displayed long-lasting antibacterial ability even up to 28 d due to the incorporation of Ag. An addition of the bioactive element Sr alleviated the potential cytotoxic effect of the excessive Ag and further facilitated the proliferation and differentiation of MC3T3-E1 osteoblast (Fig.16).

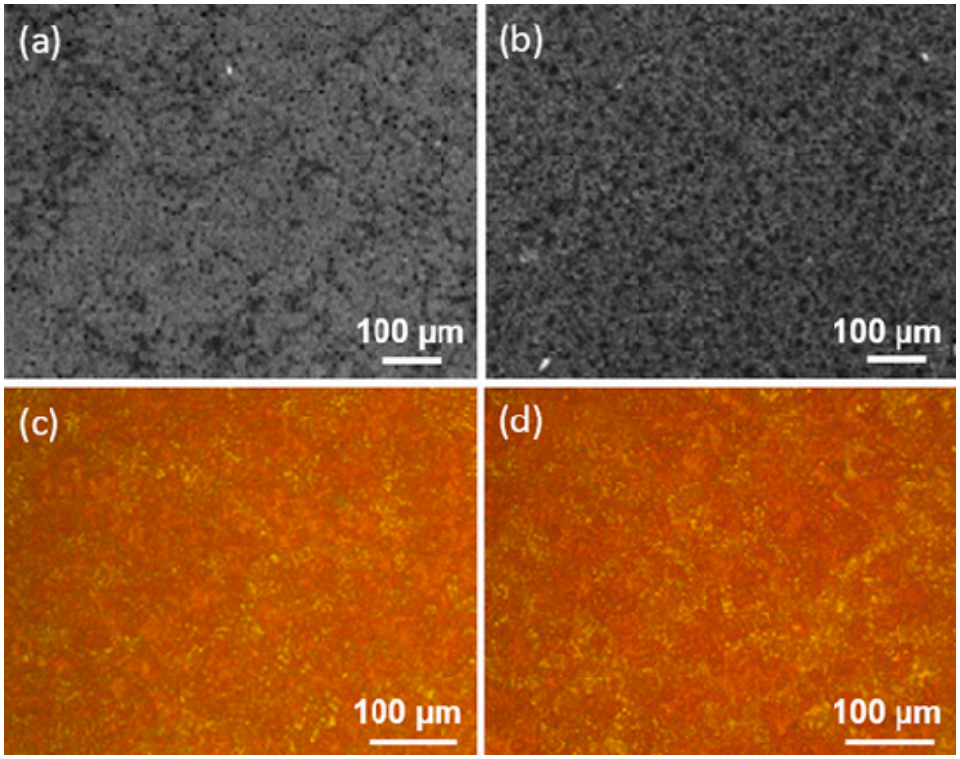

Fig.16 SEM images of MC3T3-E1 cells after culturing for 3 d and quantitative results of collagen secreted by MC3T3-E1 cells after culturing for 7 d on M-Ag0.40 (**a, c**) and M-Sr/Ag0.40 (**b, d**) indicated the bioactive element Sr are able to facilitate cell proliferation and differentiation of MC3T3-E1 osteoblast and alleviate the potential cytotoxic effect of excessive Ag [112].

3. Conclusions and future outlook

Implant-associated infections are still one of the critical issues for dental and orthopaedic implantology. The surface modification of Ti and Ti alloy seems to be a challenging strategy to prevent the development of peri-implant infection. In the present paper, MAO technique effectively and versatilely introduces inorganic antibacterial metal elements (e.g. Ag, Cu, Zn) into biomedical implants, which successfully solves the growing problem of peri-implant infection. In this mini-review, the research advance in fabrication of anti-microbial surfaces by MAO is summarized. Antibacterial metal elements were introduced into the electrolyte in the form of either metal NPs or metallic compounds.

However, the main open problems related to this strategy is that the antibacterial effect increases in a dose dependent manner, but coupled to cytotoxic behavior at the higher concentration. In fact, many Ti-based implants with strong antibacterial properties are still not available in the field of medicine, probably due to the problem mentioned above. In this review, we can also see that many studies have only focused on the development of Ti-based surfaces with effective antibacterial effect, but ignored the study of bioactivity and toxicity. Therefore, it is necessary to precisely control the content of the antibacterial metal elements and MAO parameters towards an optimal trade-off

between antibacterial properties and cytotoxicity. It is a potential way to achieve an enhancement of both antibacterial property and bioactivity directly by simultaneous addition of antibacterial metal elements and bioactive elements such as strontium (Sr), silicon(Si) in MAO electrolyte.

In addition, MAO method combined with MS was introduced to obtain desired antibacterial property and fabricate bioactive coatings in this review. Ca-P ions can be formed in the porous bio-ceramic layer on Ti surface by MAO and further transformed into crystal HA through other treatment, such as heat treatment or electrophoretic deposition. The good crystallinity of HA is conducive to cell reaction and bioactivity. Therefore, it is still a trend to develop new methods that can promote the formation of high crystallinity HA.

In conclusion, in order to overcome the toxicity concerns and guarantee the prolonging antibacterial properties, it seems to be a future research trend in the biomaterial field to add antibacterial metal elements and bioactive elements by MAO directly or assisted by other surface modification techniques such as heat treatment, hydrothermal treatment and plasma spraying in the near future. .

Acknowledgment: This work was supported by the National Natural Science Foundation of China (51671140 and 31400815), the Natural Science Foundation of Shanxi Province (2015021063), the Qualified Personnel Foundation of Taiyuan University of Technology (QPFT) (tyutrc-2011257a) and the Research Project Supported by Shanxi Scholarship Council of China (2013-030 and 2015-034).

Conflict of Interest: The authors declare that they have no conflict of interest.

References

1. Wang K (1996) The use of titanium for medical applications in the USA, Mater Sci Eng: C A213: 134-137.
2. Liu X, Chu P, Ding C (2004) Surface modification of titanium, titanium alloys, and related materials for biomedical applications, Mater Sci Eng: R: Reports 47: 49-121.
3. Pohrelyuk I, Yaskiv O, Tkachuk O, et al (2009) Formation of oxynitride layers on titanium alloys by gas diffusion treatment, Met Mater Int 15: 949-953.
4. Glinel K, Thebault P, Humblot V, et al (2012) Antibacterial surfaces developed from bio-inspired approaches, Acta Biomater 8: 1670-1684.
5. Zhao L, Wang H, Huo K, et al (2011) Antibacterial nano-structured titania coating incorporated with silver nanoparticles, Biomaterials 32: 5706-5716.
6. Donlan R M, Costerton J W (2002) Biofilms: Survival mechanisms of clinically relevant microorganisms, Clin Microbiol Rev 15: 167-193.
7. Stewart P S, William Costerton J (2001) Antibiotic resistance of bacteria in biofilms, The Lancet 358: 135-138.
8. Huang R, Han Y, Lu S (2014) Enhanced osteoblast functions and bactericidal effect of Ca and Ag dual-ion implanted surface layers on nanograined titanium alloys, J Mater Chem B 2: 4531.
9. Hetrick E M, Schoenfisch M H (2006) Reducing implant-related infections: Active release strategies, Chem Soc Rev 35: 780-789.
10. Hu H, Zhang W, Qiao Y, et al (2012) Antibacterial activity and increased bone marrow stem cell functions of Zn-incorporated TiO2 coatings on titanium, Acta Biomater 8: 904-915.
11. Esposito S, Leone S (2008) Prosthetic joint infections: Microbiology, diagnosis, management and prevention, Int J Antimicrob Agents 32: 287-293.
12. Zimmerli W (2006) Infection and musculoskeletal conditions: Prosthetic-joint-associated infections, Best Pract Res Clin Rheumatol 20: 1045-1063.
13. Tsai M-T, Chang Y-Y, Huang H-L, et al (2013) Characterization and antibacterial performance of bioactive Ti–Zn–O coatings deposited on titanium implants, Thin Solid Films 528: 143-150.
14. Bai X, Sandukas S, Appleford M, et al (2012) Antibacterial effect and cytotoxicity of Ag-doped functionally graded hydroxyapatite coatings, J Biomed Mater Res B Appl Biomater 100: 553-561.
15. Lim P N, Teo E Y, Ho B, et al (2013) Effect of silver content on the antibacterial and bioactive properties of silver-substituted hydroxyapatite, J Biomed Mater Res A 101: 2456-2464.
16. Mai L, Wang D, Zhang S, et al (2010) Synthesis and bactericidal ability of Ag/TiO2 composite films deposited on titanium plate, Appl Surf Sci 257: 974-978.

17. Chen L, Zheng L, Lv Y, et al (2010) Chemical assembly of silver nanoparticles on stainless steel for antimicrobial applications, Surf Coat Tech 204: 3871-3875.
18. Alarcon E I, Udekwu K, Skog M, et al (2012) The biocompatibility and antibacterial properties of collagen-stabilized, photochemically prepared silver nanoparticles, Biomaterials 33: 4947-4956.
19. Jia Z, Xiu P, Li M, et al (2016) Bioinspired anchoring agnps onto micro-nanoporous TiO2 orthopedic coatings: Trap-killing of bacteria, surface-regulated osteoblast functions and host responses, Biomaterials 75: 203-222.
20. Mei S, Wang H, Wang W, et al (2014) Antibacterial effects and biocompatibility of titanium surfaces with graded silver incorporation in titania nanotubes, Biomaterials 35: 4255-4265.
21. Reithofer M R, Lakshmanan A, Ping A T, et al (2014) In situ synthesis of size-controlled, stable silver nanoparticles within ultrashort peptide hydrogels and their anti-bacterial properties, Biomaterials 35: 7535-7542.
22. Wang Y, Ding X, Chen Y, et al (2016) Antibiotic-loaded, silver core-embedded mesoporous silica nanovehicles as a synergistic antibacterial agent for the treatment of drug-resistant infections, Biomaterials 101: 207-216.
23. Wu H, Zhang X, He X, et al (2014) Wear and corrosion resistance of anti-bacterial Ti–Cu–N coatings on titanium implants, Appl Surf Sci 317: 614-621.
24. Zhang X, Huang X, Jiang L, et al (2011) Surface microstructures and antimicrobial properties of copper plasma alloyed stainless steel, Appl Surf Sci 258: 1399-1404.
25. Zhang X, Huang X, Ma Y, et al (2012) Bactericidal behavior of Cu-containing stainless steel surfaces, Appl Surf Sci 258: 10058-10063.
26. Zhang X, Ma Y, Lin N, et al (2013) Microstructure, antibacterial properties and wear resistance of plasma Cu–Ni surface modified titanium, Surf Coat Tech 232: 515-520.
27. Huo K, Zhang X, Wang H, et al (2013) Osteogenic activity and antibacterial effects on titanium surfaces modified with zn-incorporated nanotube arrays, Biomaterials 34: 3467-3478.
28. Jin G, Qin H, Cao H, et al (2014) Synergistic effects of dual zn/ag ion implantation in osteogenic activity and antibacterial ability of titanium, Biomaterials 35: 7699-7713.
29. Jin G, Qin H, Cao H, et al (2015) Zn/Ag micro-galvanic couples formed on titanium and osseointegration effects in the presence of s. Aureus, Biomaterials 65: 22-31.
30. Dastjerdi R, Montazer M (2010) A review on the application of inorganic nano-structured materials in the modification of textiles: Focus on anti-microbial properties, Colloids Surf B Biointerfaces 79: 5-18.
31. He X, Li M, Wang H, et al (2015) Preparation of copper and chromium alloyed layers on pure titanium by plasma surface alloying technology, Surf Rev Lett 22: 1550056.
32. Dizaj S M, Lotfipour F, Barzegar-Jalali M, et al (2014) Antimicrobial activity of the metals and metal oxide nanoparticles, Mater Sci Eng C Mater Biol Appl 44: 278-284.
33. Rai M, Yadav A, Gade A (2009) Silver nanoparticles as a new generation of antimicrobials, Biotechnol Adv 27: 76-83.
34. Ferraris S, Spriano S (2016) Antibacterial titanium surfaces for medical implants, Mater Sci Eng C Mater Biol Appl 61: 965-978.
35. Wan Y Z, Raman S, He F, et al (2007) Surface modification of medical metals by ion implantation of silver and copper, Vacuum 81: 1114-1118.
36. Wan Y Z, Xiong G Y, Liang H, et al (2007) Modification of medical metals by ion implantation of copper, Appl Surf Sci 253: 9426-9429.
37. Cao H, Qiao Y, Liu X, et al (2013) Electron storage mediated dark antibacterial action of bound silver nanoparticles: Smaller is not always better, Acta Biomater 9: 5100-5110.
38. Necula B S, van Leeuwen J P T M, Fratila-Apachitei L E, et al (2012) In vitro cytotoxicity evaluation of porous TiO_2–Ag antibacterial coatings for human fetal osteoblasts, Acta Biomater 8: 4191-4197.
39. Lee S B, Otgonbayar U, Lee J H, et al (2010) Silver ion-exchanged sodium titanate and resulting effect on antibacterial efficacy, Surf Coat Tech 205: S172-S176.
40. García-Serrano J, Gómez-Hernández E, Ocampo-Fernández M, et al (2009) Effect of ag doping on the crystallization and phase transition of TiO_2 nanoparticles, Curr Appl Phys 9: 1097-1105.
41. Meng F, Sun Z (2009) A mechanism for enhanced hydrophilicity of silver nanoparticles modified TiO2 thin films deposited by rf magnetron sputtering, Appl Surf Sci 255: 6715-6720.

42. Tian X B, Wang Z M, Yang S Q, et al (2007) Antibacterial copper-containing titanium nitride films produced by dual magnetron sputtering, Surf Coat Tech 201: 8606-8609.
43. Li B, Liu X, Meng F, et al (2009) Preparation and antibacterial properties of plasma sprayed nano-titania/silver coatings, Mater Chem Phys 118: 99-104.
44. Mungkalasiri J, Bedel L, Emieux F, et al (2009) Dli-cvd of TiO2–Cu antibacterial thin films: Growth and characterization, Surf Coat Tech 204: 887-892.
45. Sul Y T, Kang B S, Johansson C, et al (2009) The roles of surface chemistry and topography in the strength and rate of osseointegration of titanium implants in bone, J Biomed Mater Res A 89: 942-950.
46. Wei D, Zhou Y, Yang C (2009) Structure, cell response and biomimetic apatite induction of gradient TiO2-based/nano-scale hydrophilic amorphous titanium oxide containing ca composite coatings before and after crystallization, Colloids Surf B Biointerfaces 74: 230-237.
47. Yan J, Sun J F, Chu P K, et al (2013) Bone integration capability of a series of strontium-containing hydroxyapatite coatings formed by micro-arc oxidation, J Biomed Mater Res A 101: 2465-2480.
48. Zhao B H, Lee I S, Han I H, et al (2007) Effects of surface morphology on human osteosarcoma cell response, Curr Appl Phys 7: e6-e10.
49. Sun J, Han Y, Cui K (2008) Microstructure and apatite-forming ability of the mao-treated porous titanium, Surf Coat Tech 202: 4248-4256.
50. Miao S, Cheng K, Weng W, et al (2008) Fabrication and evaluation of Zn containing fluoridated hydroxyapatite layer with zn release ability, Acta Biomater 4: 441-446.
51. Wang Y, Yu H, Chen C, et al (2015) Review of the biocompatibility of micro-arc oxidation coated titanium alloys, Mater Design 85: 640-652.
52. Matykina E, Arrabal R, Skeldon P, et al (2009) Transmission electron microscopy of coatings formed by plasma electrolytic oxidation of titanium, Acta Biomater 5: 1356-1366.
53. Wan L, Li J F, Feng J Y, et al (2007) Anatase TiO2 films with 2.2ev band gap prepared by micro-arc oxidation, Mater Sci Eng: B 139: 216-220.
54. Cheng Y L, Wu X Q, Xue Z G, et al (2013) Microstructure, corrosion and wear performance of plasma electrolytic oxidation coatings formed on ti–6al–4v alloy in silicate-hexametaphosphate electrolyte, Surf Coat Tech 217: 129-139.
55. Necula B S, Fratila-Apachitei L E, Zaat S A, et al (2009) In vitro antibacterial activity of porous TiO2-Ag composite layers against methicillin-resistant staphylococcus aureus, Acta Biomater 5: 3573-3580.
56. Necula B S, Apachitei I, Tichelaar F D, et al (2011) An electron microscopical study on the growth of TiO2-ag antibacterial coatings on ti6al7nb biomedical alloy, Acta Biomater 7: 2751-2757.
57. Yao X, Zhang X, Wu H, et al (2014) Microstructure and antibacterial properties of Cu-doped TiO2 coating on titanium by micro-arc oxidation, Appl Surf Sci 292: 944-947.
58. Song W H, Ryu H S, Hong S H (2009) Antibacterial properties of ag (or pt)-containing calcium phosphate coatings formed by micro-arc oxidation, J Biomed Mater Res A 88: 246-254.
59. Muhaffel F, Cempura G, Menekse M, et al (2016) Characteristics of multi-layer coatings synthesized on ti6al4v alloy by micro-arc oxidation in silver nitrate added electrolytes, Surf Coat Tech 307: 308-315.
60. Teker D, Muhaffel F, Menekse M, et al (2015) Characteristics of multi-layer coating formed on commercially pure titanium for biomedical applications, Mater Sci Eng C Mater Biol Appl 48: 579-585.
61. Chang C, Huang X, Liu Y, et al (2015) High-current anodization: A novel strategy to functionalize titanium-based biomaterials, Electrochim Acta 173: 345-353.
62. Huang X, Liu Y, Yu H, et al (2016) One-step fabrication of cytocompatible micro/nano-textured surface with TiO2 mesoporous arrays on titanium by high current anodization, Electrochim Acta 199: 116-125.
63. Zhu W, Zhang Z, Gu B, et al (2013) Biological activity and antibacterial property of nano-structured TiO2 coating incorporated with cu prepared by micro-arc oxidation, J Mater Sci Technol 29: 237-244.
64. Zhang L, Guo J, Huang X, et al (2016) The dual function of cu-doped TiO2coatings on titanium for application in percutaneous implants, J Mater Chem B 4: 3788-3800.
65. Zhang X, Wang H, Li J, et al (2016) Corrosion behavior of Zn-incorporated antibacterial TiO2 porous coating on titanium, Ceram Int. doi:10.1016/j.ceramint.2016.07.220.
66. Zhang L, Gao Q, Han Y (2016) Zn and ag co-doped anti-microbial TiO2 coatings on Ti by micro-arc oxidation, J Mater Sci Technol 32: 919-924.
67. Yeo S Y, Jeong S H (2003) Preparation and characterization of polypropylene/silver nanocomposite fibers, Polym Int 52: 1053-1057.

68. Zinjarde S (2012) Bio-inspired nanomaterials and their applications as antimicrobial agents, Chronicles of Young Scientists 3: 74.
69. Sondi I, Salopek-Sondi B (2004) Silver nanoparticles as antimicrobial agent: A case study on e. Coli as a model for gram-negative bacteria, J Colloid Interface Sci 275: 177-182.
70. Yun H, Kim J D, Choi H C, et al (2013) Antibacterial activity of cnt-Ag and go-Ag nanocomposites against gram-negative and gram-positive bacteria, B Korean Chem Soc 34: 3261-3264.
71. Iavicoli I, Fontana L, Leso V, et al (2013) The effects of nanomaterials as endocrine disruptors, Int J Mol Sci 14: 16732-16801.
72. Morones J R, Elechiguerra J L, Camacho A, et al (2005) The bactericidal effect of silver nanoparticles, Nanotechnology 16: 2346-2353.
73. Jo Y-K, Kim B H, Jung G (2009) Antifungal activity of silver ions and nanoparticles on phytopathogenic fungi, Plant Dis 93: 1037-1043.
74. Cao H, Liu X (2013) Activating titanium oxide coatings for orthopedic implants, Surf Coat Tech 233: 57-64.
75. Macomber L, Imlay J A (2009) The iron-sulfur clusters of dehydratases are primary intracellular targets of copper toxicity, Proc Natl Acad Sci U S A 106: 8344-8349.
76. M Raffi S M, TM Bhatti, JI Akhter, A Hameed, W Yawar, MM Hasan (2010) Investigations into the antibacterial behavior of copper nanoparticles against escherichia coli, Ann Microbiol 60: 75-80.
77. Usman M S, El Zowalaty M E, Shameli K, et al (2013) Synthesis, characterization, and antimicrobial properties of copper nanoparticles, Int J Nanomedicine 8: 4467-4479.
78. HL Pape F S, P Contini, C Devillers, A Maftah, P Leprat (2002) Evaluation of the anti-microbial properties of an activated carbon fibre supporting silver using a dynamic method, Carbon 40: 2947–2954.
79. Mahapatra O, Bhagat M, Gopalakrishnan C, et al (2008) Ultrafine dispersed cuo nanoparticles and their antibacterial activity, Journal of Experimental Nanoscience 3: 185-193.
80. Li L H, Kong Y M, Kim H W, et al (2004) Improved biological performance of Ti implants due to surface modification by micro-arc oxidation, Biomaterials 25: 2867-2875.
81. Zhao Z, Chen X, Chen A, et al (2009) Synthesis of bioactive ceramic on the titanium substrate by micro-arc oxidation, J Biomed Mater Res A 90: 438-445.
82. Song W H, Jun Y K, Han Y, et al (2004) Biomimetic apatite coatings on micro-arc oxidized titania, Biomaterials 25: 3341-3349.
83. Sun J, Han Y, Huang X (2007) Hydroxyapatite coatings prepared by micro-arc oxidation in Ca- and P-containing electrolyte, Surf Coat Tech 201: 5655-5658.
84. Chen W, Liu Y, Courtney H S, et al (2006) In vitro anti-bacterial and biological properties of magnetron co-sputtered silver-containing hydroxyapatite coating, Biomaterials 27: 5512-5517.
85. BD Boyan R B, K Kieswetter, Y Liu, D L Cochran, S Szmuckler-Moncler, DD Dean, Z.Schwartz (1998) Titanium surface roughness alters responsiveness of mg63 osteoblast-like cells to 1α,25-(oh)2d3, journal of biomedical materials 77-85.
86. Naveena N, Venugopal J, Rajeswari R, et al (2012) Biomimetic composites and stem cells interaction for bone and cartilage tissue regeneration, J Mater Chem 22: 5239.
87. Jamuna-Thevi K, Bakar S A, Ibrahim S, et al (2011) Quantification of silver ion release, in vitro cytotoxicity and antibacterial properties of nanostuctured Ag doped TiO2 coatings on stainless steel deposited by rf magnetron sputtering, Vacuum 86: 235-241.
88. Brammer K S, Oh S, Cobb C J, et al (2009) Improved bone-forming functionality on diameter-controlled tio(2) nanotube surface, Acta Biomater 5: 3215-3223.
89. Oh S, Daraio C, Chen L H, et al (2006) Significantly accelerated osteoblast cell growth on aligned TiO2 nanotubes, J Biomed Mater Res A 78: 97-103.
90. Wilmowsky C, Bauer S, Lutz R, et al (2009) In vivo evaluation of anodic TiO2 nanotubes: An experimental study in the pig, J Biomed Mater Res B Appl Biomater 89: 165-171.
91. Gao A, Hang R, Huang X, et al (2014) The effects of titania nanotubes with embedded silver oxide nanoparticles on bacteria and osteoblasts, Biomaterials 35: 4223-4235.
92. Kim M S, Ryu J J, Sung Y M (2007) One-step approach for nano-crystalline hydroxyapatite coating on titanium via micro-arc oxidation, Electrochem Commun 9: 1886-1891.
93. Ni J H, Shi Y L, Yan FY, et al (2008) Preparation of hydroxyapatite-containing titania coating on titanium substrate by micro-arc oxidation, Mater Res Bull 43: 45-53.

94. Y Han D C, JF Sun, YM Zhang, KW Xu (2008) Uv-enhanced bioactivity and cell response of micro-arc oxidized titania coatings, Acta Biomater 4: 1518-1529.
95. Hang R, Gao A, Huang X, et al (2014) Antibacterial activity and cytocompatibility of cu-ti-o nanotubes, J Biomed Mater Res A 102: 1850-1858.
96. Zong M, Bai L, Liu Y, et al (2017) Antibacterial ability and angiogenic activity of Cu-Ti-O nanotube arrays, Mater Sci Eng: C 71: 93-99.
97. Burghardt I, Luthen F, Prinz C, et al (2015) A dual function of copper in designing regenerative implants, Biomaterials 44: 36-44.
98. Ramaswamy Y, Wu C, Zhou H, et al (2008) Biological response of human bone cells to zinc-modified Ca-Si-based ceramics, Acta Biomater 4: 1487-1497.
99. Raghupathi K R, Koodali R T, Manna A C (2011) Size-dependent bacterial growth inhibition and mechanism of antibacterial activity of zinc oxide nanoparticles, Langmuir 27: 4020-4028.
100. Boyd D, Li H, Tanner D A, et al (2006) The antibacterial effects of zinc ion migration from zinc-based glass polyalkenoate cements, J Mater Sci Mater Med 17: 489-494.
101. Wu C, Ramaswamy Y, Chang J, et al (2008) The effect of Zn contents on phase composition, chemical stability and cellular bioactivity in zn-ca-si system ceramics, J Biomed Mater Res B Appl Biomater 87: 346-353.
102. Ibănescu M, Muşat V, Textor T, et al (2014) Photocatalytic and antimicrobial Ag/ZnO nanocomposites for functionalization of textile fabrics, J Alloy Compd 610: 244-249.
103. Li J, Liu X, Qiao Y, et al (2014) Antimicrobial activity and cytocompatibility of Ag plasma-modified hierarchical TiO2 film on titanium surface, Colloids Surf B Biointerfaces 113: 134-145.
104. Mohapatra S (2014) Tunable surface plasmon resonance of silver nanoclusters in ion exchanged soda lime glass, J Alloy Compd 598: 11-15.
105. Kim T, Yoshitake M, Yagyu S, et al (2010) Xps study on band alignment at pt o-terminated zno(0001) interface, Surf Interface Anal 42: 1528-1531.
106. Carvalho P, Sampaio P, Azevedo S, et al (2014) Influence of thickness and coatings morphology in the antimicrobial performance of zinc oxide coatings, Appl Surf Sci 307: 548-557.
107. Cao H, Liu X, Meng F, et al (2011) Biological actions of silver nanoparticles embedded in titanium controlled by micro-galvanic effects, Biomaterials 32: 693-705.
108. Bai L, Hang R, Gao A, et al (2015) Nanostructured titanium–silver coatings with good antibacterial activity and cytocompatibility fabricated by one-step magnetron sputtering, Appl Surf Sci 355: 32-44.
109. Gao A, Hang R, Chu P K (2016) Recent advances in anti-infection surfaces fabricated on biomedical implants by plasma-based technology, Surf Coat Tech. doi:10.1016/j.surfcoat.2016.04.020.
110. Zhang X, Hang R, Wu H, et al (2013) Synthesis and antibacterial property of Ag-containing TiO2 coatings by combining magnetron sputtering with micro-arc oxidation, Surf Coat Tech 235: 748-754.
111. Zhang X, Wu H, Geng Z, et al (2014) Microstructure and cytotoxicity evaluation of duplex-treated silver-containing antibacterial tio(2) coatings, Mater Sci Eng C Mater Biol Appl 45: 402-410.
112. He X, Zhang X, Bai L, et al (2016) Antibacterial ability and osteogenic activity of porous Sr/Ag-containing TiO2 coatings, Biomed Mater 11: 045008.